

# Consideration of the nonlinear viscoelasticity of PVB through a Time-Strain Superposition

## Authors

Main Author:

Dr.-Ing. Miriam Schuster  
TU Darmstadt - Institute of Structural  
Mechanics and Design – Glass Competence  
Center  
Tel.: +49 6151 16-23014  
E-mail: schuster@ismd.tu-darmstadt.de  
ORCID: 0000-0001-7975-9535

M.Eng. Kerstin Thiele

TU Darmstadt - Institute of Structural  
Mechanics and Design – Glass Competence  
Center  
Tel.: +49 6151 16-23014  
E-mail: thiele@ismd.tu-darmstadt.de  
ORCID: 0000-0003-0579-7859

Prof. Dr.-Ing. Jens Schneider

TU Darmstadt - Institute of Structural  
Mechanics and Design – Glass Competence  
Center  
Tel.: +49 6151 16-23013  
E-mail: schneider@ismd.tu-darmstadt.de  
ORCID: 0000-0003-2680-9628

## Keywords

Laminated safety glass, Interlayer, Nonlinear viscoelasticity, Time-Strain Superposition

## Abstract

The use of laminated safety glass enables residual load-bearing capacity after fracture of the glass panes. The acting load is carried by the glass fragments (adhering to the interlayer) and the interlayer itself. The interlayer locally delaminates from the glass and experiences large strains. Hence, to numerically describe the post-fracture behaviour of laminated safety glass, nonlinear (strain dependent) viscoelastic material behaviour has to be taken into account for the interlayer.

The most used laminated glass interlayer is polyvinylbutyral (PVB). For this, the viscoelastic material behaviour in the linear range (Prony parameters of the generalized Maxwell model and Time-Temperature Superposition Principle TTSP) and the linearity limits, which characterize the transition from linear viscoelastic to nonlinear viscoelastic material behaviour, are well described in literature. This paper investigates the viscoelastic

behaviour at strain magnitudes exceeding the linearity limits. For this purpose, relaxation tests in uniaxial tensile mode are carried out on the interlayer material. During the tests a high deviation from linear viscoelastic behaviour is observed.

The Schapery model, which extends the linear viscoelastic constitutive law with strain-dependent nonlinearity factors, is often used in literature to describe nonlinear viscoelastic material behaviour. The nonlinearity factors, which include a Time-Strain Superposition Principle (TSSP), were investigated to create a mastercurve.

## 1 Introduction

In order to design laminated (safety) glass, information about the material behaviour of the polymeric interlayer is of interest. In the intact state of the laminate, shear forces are transmitted via the interlayer which results in a shear coupling effect.

The identification of the temperature dependent linear viscoelastic material behaviour of PVB interlayers is done by Dynamic Mechanical Thermal Analysis (DMTA) as described in [15]. As a result, a Prony series and Time-Temperature Superposition Principles are obtained.

In recent years, there has been an increasing interest in studying the behaviour of laminated (safety) glass after glass fracture. In this state the interlayer partially delaminates from the glass fragments and undergoes large deformations exceeding the linearity limits, between the fragments. The film is then mainly subjected to tensile stress [9, 12].

To be able to describe the post-fracture behaviour of the entire laminate, the description of the PVB material at large deformations is of interest. Therefore, tensile relaxation tests were performed on interlayer material at different temperatures and strain levels at constant relative humidity. Saflex® RB41 [16] was chosen for the investigations and will be hereafter referred to as PVB.

## 2 Viscoelasticity

Subjecting a material with a viscoelastic material behaviour to a constant strain level  $\gamma_0$  or  $\epsilon_0$ , the stress response  $\tau(t)$  resp.  $\sigma(t)$  results to be decaying with time. Such tests are called relaxation tests. The ratio of stress and strain

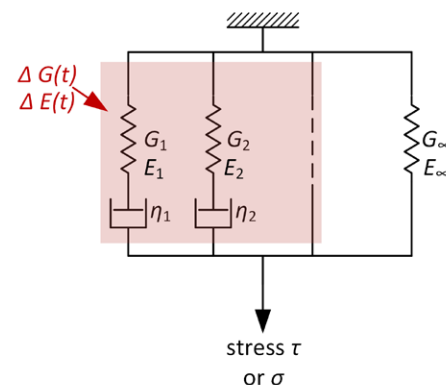


Fig. 1: Generalized Maxwell model. The red marked area represents the transient material behaviour.

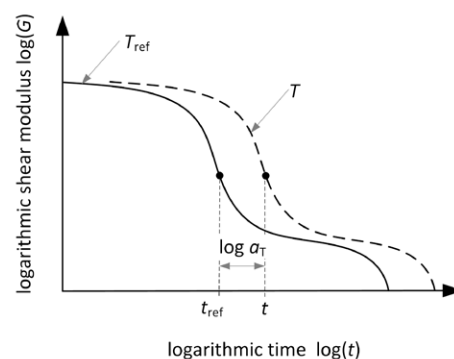


Fig. 2: Time-Temperature Superposition Principle for thermorheological simple material behaviour.

is the relaxation function  $G(t) = \tau(t)/\gamma_0$  resp.  $E(t) = \sigma(t)/\epsilon_0$ . After sufficient amount of time  $G_\infty$  resp.  $E_\infty$  is approached. Hence, the relaxation function can be split into a time invariant ( $G_\infty$  resp.  $E_\infty$ ) and a transient part ( $\Delta G$  resp.  $\Delta E$ ), see Eq. (1). For thermoplastics  $G_\infty$  resp.  $E_\infty$  is usually zero [8].

$$G(t) = G_\infty + \Delta G(t) \quad E(t) = E_\infty + \Delta E(t) \quad (1)$$

In intact laminated safety glass, the deformations of the interlayer are relatively small and linear viscoelastic material behaviour is often assumed [13]. The Generalized Maxwell model (Figure 1) is commonly used to describe linear viscoelasticity. Mathematically, this model is expressed by a so-called Prony series. The Prony parameters have to be determined experimentally e.g., with DMTA or relaxation tests at small strains. The relaxation function of linear viscoelastic materials is independent on the applied strain level. The origin of the relaxation behaviour

of polymers lies in the mobility of the molecular chains [8]. This mobility can be activated thermally, which means that a higher temperature leads to faster and a lower temperature to slower relaxation. For thermorheologically simple materials, simple mathematical relationships exist between loading duration and temperature. These are called Time-Temperature Superposition Principles (TTSP) and allow the determination of the material behaviour at long loading durations by relatively short tests at elevated temperatures. As already mentioned, the temperature change essentially influences the relaxation time. Graphically, this means that the relaxation curves at  $T$  and at  $T_{ref}$  in the log-log plot differ essentially by a shift on the horizontal axis, see Figure 2.

The horizontal distance between the two curves is referred to as  $\log a_T$ . Thus, multiplying the times of a test conducted at the reference temperature  $T_{ref}$  by the corresponding shift factor  $a_T$ , leads to the same result as a relaxation test conducted at temperature  $T$ .

If strain is applied in the relaxation test that exceeds the linearity limits, the applied strain level influences the relaxation function and nonlinear viscoelastic material models become necessary. Detailed investigations of the linearity limits on the investigated material have already been published by the authors in [18]. It can be summarized, that the linearity limits are dependent on time resp. frequency and temperature. In other words: A high linear viscoelastic modulus results in a low linearity limit, while a low linear viscoelastic modulus results in a high linearity limit.

The linearity limit is exceeded at the latest in the post-fracture state, where the interlayer is mainly subjected to tensile stress. In a first approximation the tensile stress is considered to be uniaxial, hence, the nonlinear viscoelastic considerations subsequently refer to uniaxial tension.

One of the most flexible nonlinear viscoelastic material models is Schapery's single integral approach [1, 3, 2]. This model consists of the generalized Maxwell model  $(E_\infty, E_0, \Delta E)$ , supplemented by four different nonlinearity functions  $h_\infty(\epsilon)$ ,  $h_1(\epsilon)$ ,  $h_2(\epsilon)$  and  $a_\epsilon(\epsilon)$ . For single step relaxation tests with constant strain levels  $\epsilon_0$  and using the Prony series for the linear viscoelastic behaviour, Eq. (2) or Eq. (3) are obtained. In single step relaxation tests, the nonlinearity factors  $h_1$  and  $h_2$  cannot be determined separately. Instead, they are combined to  $h_{1,2}(\epsilon) = h_1(\epsilon) \cdot h_2(\epsilon)$  resp.  $h^*_{1,2}(\epsilon) \neq h_{1,2}(\epsilon)$ .

$$E(t) = h_\infty(\epsilon) E_\infty + h_{1,2}(\epsilon) \left( \sum_{i=1}^N E_i \cdot \exp\left(-\frac{t}{a_\epsilon \cdot \tau_i}\right) \right) \quad (2)$$

$$E(t) = h_0(\epsilon) E_0 + h^*_{1,2}(\epsilon) \left( \sum_{i=1}^N E_i \cdot \left(1 - \exp\left(-\frac{t}{a_\epsilon \cdot \tau_i}\right)\right) \right) \quad (3)$$

If the nonlinearity functions equal to unity, the relaxation curve corresponds to the linear viscoelastic Prony series. Hence, the same model can be used for both, the linear and nonlinear range, which is the biggest advantage of this model.

If  $h_\infty = h_{1,2} = 1$  or  $h_0 = h^*_{1,2} = 1$ , Knauss and Emris model published in [4] is obtained. This model is based on the free volume theory and states that an increased strain leads to an increased free volume, which in turn accelerates the relaxation process. Hence, a strain increase has a similar effect than a temperature increase. Both lead to a horizontal shift of the relaxation curve to lower times. Analogously to the TTSP function, this shift is called Time-Strain or Time-Stress Superposition Principle (TSSP).

The influence of  $h_\infty$  and  $h_{1,2}$  or  $h_0$  and  $h^*_{1,2}$  is best described with a linear y-scale.  $h_0$  resp.  $h_\infty \neq 1$  affects the time-invariant part of the relaxation function. It shifts the Prony series vertically along the y-axis.  $h_{1,2}$  or  $h^*_{1,2}$  modifies the height of the stiffness drop with time, which results in a change of the relaxation curve shape. In log-log scale,  $h_\infty = h_{1,2}$  or  $h(\epsilon) = h_0 = h^*_{1,2}$  and  $a_\epsilon = 1$ , shifts the Prony series purely vertically.

Again, in the nonlinear viscoelastic range, temperature affects the relaxation behaviour of the polymeric interlayers. In [3] it is stated that the temperature dependent material behaviour can be considered by adding  $T$  as an argument of the strain-dependent factor  $a_\epsilon = a_\epsilon(\epsilon, T)$ . In [8] and [6] a method is presented, where the TTSP and TSSP are combined via multiplication of the individual shift factors  $a_{\epsilon,T} = a_\epsilon \cdot a_T$  resp. addition of the logarithmic shift factors  $\log a_{\epsilon,T} = \log a_\epsilon + \log a_T$ . This method is simple and will be followed in this paper. However, this neglects nonlinear interaction of strain and temperature effects in the case of simultaneous occurrence.

In [5],[10], it is also indicated that the TTSP remains valid in the nonlinear viscoelastic region. However, in those publications, the TTSP is not applied to curves of the same strain or stress level, but to curves with the same percentage of stress exceeding the yield stress.

### 3 Uniaxial tensile relaxation tests at various strain levels

#### 3.1 Description of experimental settings

The relaxation behaviour of PVB was studied in uniaxial relaxation tests with different strain levels at different temperatures and constant relative humidity. The different strain levels were applied displacement controlled with a constant rate of 400mm/min and then kept constant for the test duration of at least 1h. The tests were performed in a ZWICK ROELL Z050 universal testing machine. The test

climate was controlled by surrounding the test area with a climate chamber.

The interlayer to be examined was sent air sealed to the institute by the manufacturer in foils of approx. DIN A4 size with a nominal thickness of 0.76mm. Before cutting the specimen, the film was heated to 100°C for approx. 1h to avoid subsequent shrinkage during the tests. After that, the specimens (Becker tensile bars [11] or rectangular specimens) were punched out or cut with scissors, respectively. The specimens were then stored for at least 4h in the test climate (50%rH and different temperatures).

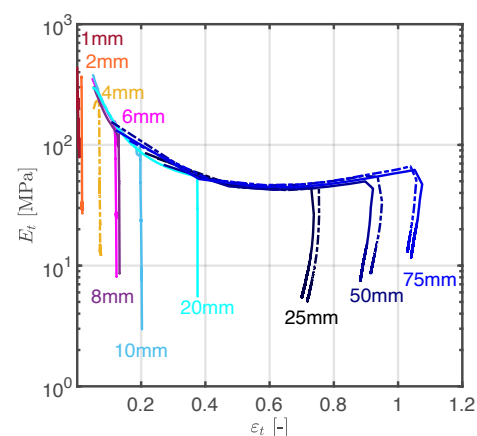


Fig. 3: True tensile secant modulus  $E_T$  [Eq. (6)] in dependence of true strain  $\epsilon_t$  [Eq. (5)] for a temperature of  $T = 0^\circ\text{C}$ .

Prior to specimen mounting, the thickness of the specimens was measured in at least three locations using a digital micrometer and a gray scale pattern was applied to the specimen. The gray scale pattern was marked with a black pen from STAEDTLER [19] in size S and allows the placement of four virtual gauges that can be tracked with the DIC software ISI-SYS VIC GAUGE 2D [17] to check the constancy of the applied strain level. To ensure good lighting conditions, LED strips were installed in the climate chamber. In addition, white paper was positioned behind the specimen so that the measurement of the transparent specimen cannot be disturbed by the fan of the climate chamber behind it. Since the climate chamber has only a narrow window, only one camera could be used. It had to be aligned so that it was perpendicular to the specimen. Two of the gauges are placed vertically on top of each other. The connection of these two gauges creates an extensometer that measures longitudinal engineering strain. The other two gauges are located horizontally next to each other. This extensometer measures the transverse engineering strain. The force decrement was measured with a load cell. Details in the experimental procedure differ depending on whether small/medium or large

strains were applied. The classification into small/medium or large strain was made based on the true stress-strain diagram or the true secant modulus-strain diagram (Figure 3). As long as the secant modulus decreases with increasing strain, we speak of small/medium strain. When the secant modulus increases again, we speak of large strain. The differences in the experimental procedure are explained below.

#### 3.1.1 Large strain relaxation tests

For the tests with large strains, Becker [11] tensile bars (Figure 4) were used as specimen geometry. This geometry prevents premature failure at the clamping point. The samples were punched from the foil. Hydraulic jaws were used to clamp the specimen in the universal testing machine. To be able to apply the largest possible deformations, the built-in 50kN load cell was used. The load cell was manually synchronized with the DIC measurement.

Three different strain levels were investigated for three different temperatures (0°C: energy elastic range, 20°C:  $\approx$  glass transition range and 40°C: entropy elastic range [18]). At 0°C, displacements of 25mm, 50mm and 75mm have been applied, at 20°C 50mm, 100mm and 125mm and at 40°C 50mm, 100mm and 150mm.

The test set-up, placement of the gauges before and during the relaxation test are shown in Figure 5.

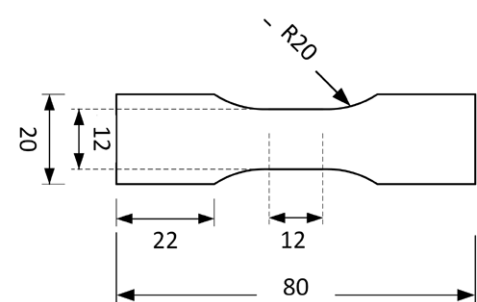


Fig. 4: Becker tensile bar. Dimensions in [mm].

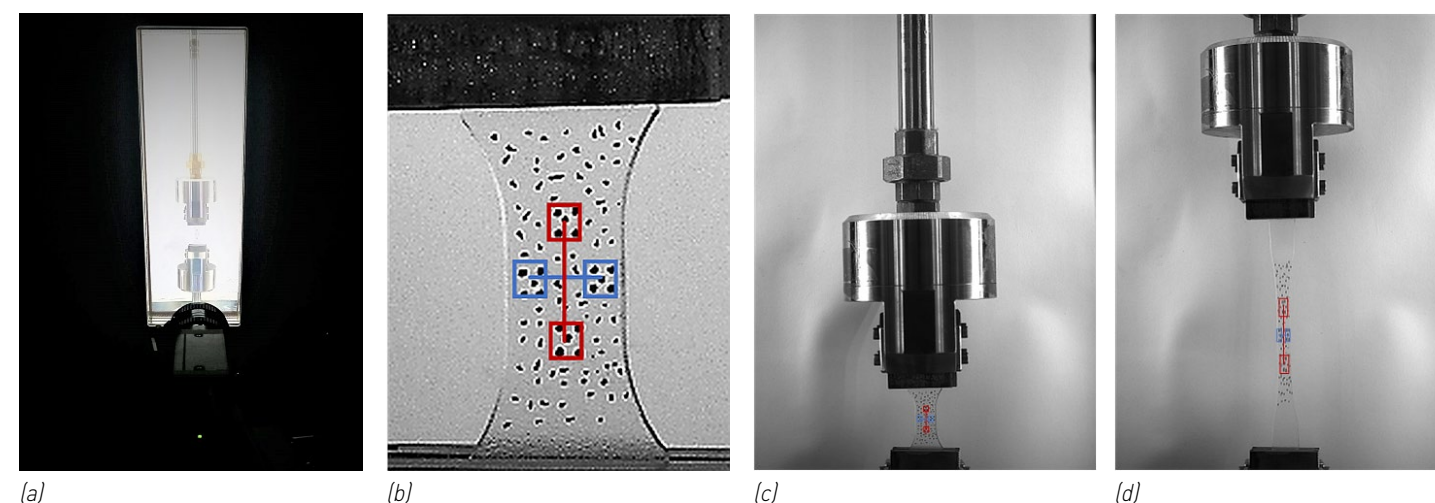


Fig. 5: (a) Test set-up, (b) gauges and extensometers, (c) sample before test start and (d) sample during relaxation test.

T [°C]	w [mm]	$\epsilon_t$ [%]	Geometry	Nb. of samples
0	1	0.5	rect.	1
0	2	1.6, 1.8	rect.	2a
0	4	7.2	rect.	1
0	6	12.3	rect.	1
0	8	13.3	rect.	1
0	10	20.2	rect.	1
0	20	37.6	rect.	1
0	25	70.8, 72.4	Becker	2
0	50	88.7, 92.0	Becker	2
0	75	104.4, 103.3, 97.5	Becker	3
20	50	80.9, 83.4	Becker	2
20	100	107.1, 102.1	Becker	2
20	125	117.2, 116.5, 114.6	Becker	3
40	50	94.8, 96.8	Becker	2
40	100	123.3, 127.8	Becker	2
40	150	146.1, 144.8, 152.2	Becker	3

a mean value of both tests were used for further evaluation.

Table 1: List of tensile relaxation tests at 50%rH. Temperature  $T$ , displacement  $w$ , mean of true strain  $\epsilon_t$ , geometry of the specimen and number of experiments are listed.

#### 3.1.2 Small to medium strain relaxation tests

For the tests with small to medium strains, rectangular specimens and simple toothed clamps made of steel were used as shown in Figure 6 and Figure 7(a). The rectangular specimens were cut out by hand with scissors. The total length of one specimen is 120mm. At both sides 40mm are used to clamp the specimen, the initial test length  $l_0$  is 40mm. The specimens were clamped firmly with one screw on each side. Therefore, two holes in the specimen were needed, see Figure 6. The specimen together with the clamps were then installed in the climate chamber and the universal testing machine (Figure 7(b)). An

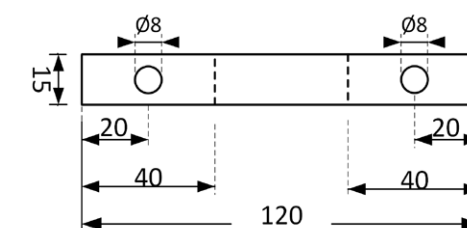


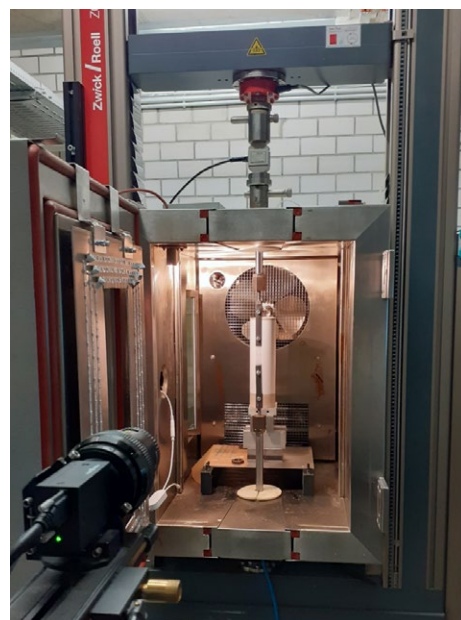
Fig. 6: Rectangular sample. Dimensions in [mm].

additional load cell load cell (2kLB  $\approx$  8.9kN) was installed to record data synchronized with the camera. Seven different strain levels (displacement levels of 1, 2, 4, 6, 8, 10 and 20mm) were

investigated for 0°C and 50%rH ranging from small to medium large strains, see Table 1. The relaxation test at 1mm displacement level was the smallest possible test in this test setup that led to a meaningful evaluation. The relaxation tests at displacement level 2mm showed good agreement. The relaxation tests at a displacement level of 20mm showed good agreement with the smallest strain level of the large strain tests at same test conditions, suggesting that the experimental setups are comparable.



(a)



(b)

Fig. 7: (a) Toothed clamps made of steel and (b) test set up.

### 3.2 Evaluation of secant modulus and mastercurve

During the relaxation tests, force and displacement data from the universal testing machine were recorded. In addition, technical strain data in x (longitudinal) and y (transverse) direction were recorded via digital image correlation.

A distinction between engineering (Eq. (4)) and true stress/strain (Eq. (5)) values is done. While the engineering values refer to the initial geometry, the true values refer to the actual geometry of the samples.  $\nu$  corresponds to the Poisson ratio.

$$\epsilon = \frac{\Delta l}{l_0} \quad \sigma = \frac{F}{A_0} \quad (4)$$

$$\epsilon_t = \ln(1 + \epsilon) \quad \sigma_t = \sigma \cdot (1 + \epsilon)^{2\nu} \quad \nu = -\frac{\epsilon_{t,y}}{\epsilon_{t,x}} \quad (5)$$

The relaxation functions were calculated with the true stress  $\sigma_t(t)$  and the strain  $\epsilon_t(t) \approx \text{constant}$ . This corresponds to the secant Youngs modulus:

$$E_t(t) = \frac{\sigma_t(t)}{\epsilon_t(t)} \quad (6)$$

Since the deformation can not be applied suddenly, the withdrawn DIN 53441 [21] recommends to start the evaluation of the relaxation tests at a time  $t^*$  that corresponds to  $t^* = 10t_0$  (see Figure 8), wherein  $t_0$  is the time required to apply the strain level, in order to neglect an influence of the loading history. In order to compare the linear viscoelastic Prony series with the tensile relaxation tests, the shear modulus is approximately converted into Youngs modulus. For this purpose, the Poisson's ratio is assumed to be  $\nu = 0.5$  [22], which leads to Eq. (7).

$$G \approx \frac{E}{3} \quad (7)$$

However, this is only an approximation, since the Poisson ratio  $\nu$  varies with temperature and time/frequency and typically lies between 0.3 (in the energy elastic range) and 0.5 (in the entropy-elastic range) [13].

The TTSP of [18] is used without any modifications. In addition, Time-Strain Superposition is investigated. The horizontal shifting procedure is similar to the one for TTSP described in [14]. A specially created Matlab [20] script is used, which compares two relaxation curves at different strain levels with each other. First, the overlap range on the y-axis of both curves is determined. Subsequently, the horizontal distance in the overlap area is minimized using a least squares algorithm. For this reason, the times of the curve to be shifted are multiplied by the factor  $a_\epsilon$ . The factor  $a_\epsilon$  is varied until the objective function  $f$  in Eq. (8) has reached its minimum.  $t_{\text{ref},i}$  and  $t_{\epsilon,i}$  are defined such as  $G_{\text{ref}}(t_{\text{ref},i}) = G_\epsilon(t_i)$ .

$$f = \sum_{i \in \text{overlap range}} (t_{\text{ref},i} - t_{\epsilon,i} \cdot a_\epsilon)^2 \quad (8)$$

### 3.3 Test results

Before and immediately after the test, the specimen outlines were roughly recorded with a pen. Figure 9 shows two specimens after the relaxation tests at 0°C and 75mm as well as 0°C and 8mm elongation. After some

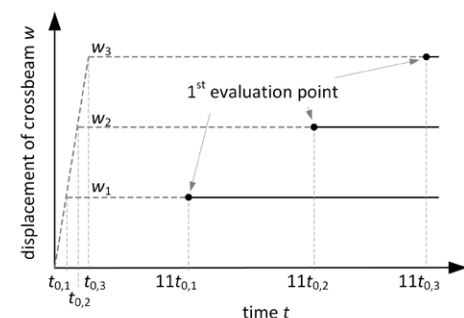
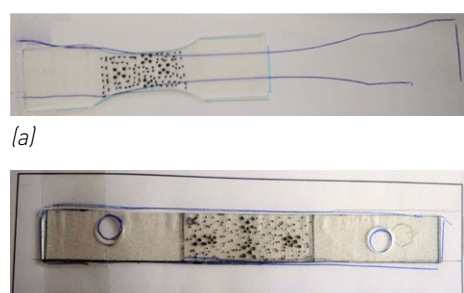


Fig. 8: Uniaxial tensile relaxation test program.

time, the specimens have returned to their original geometry (before test), so that plastic deformations are excluded.

In the following sections the relaxation curves observed in the relaxation tests of large strain as well as of small to medium large strain are shown.



(a)

Fig. 9: (a) Sample after large strain relaxation test (0°C, 75mm) and (b) after medium strain relaxation test (0°C, 8mm).

### 3.3.1 Large strain relaxation tests

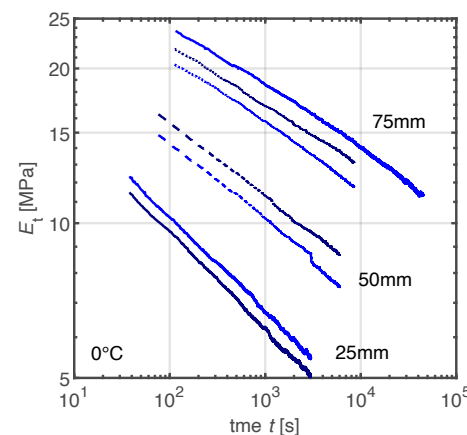
Figure 10 shows the relaxation function (calculated with true stress and strain data) for the three investigated temperatures 0°C, 20°C and 40°C. In all cases, higher strain levels lead to stiffer material behaviour. This fits well with the curves of true tensile modulus during load application, see Figure 3. The comparison of the relaxation curves for 50mm displacements at different temperatures shows, as expected, that higher temperatures result in lower stiffness.

### 3.3.2 Small to medium strain relaxation tests

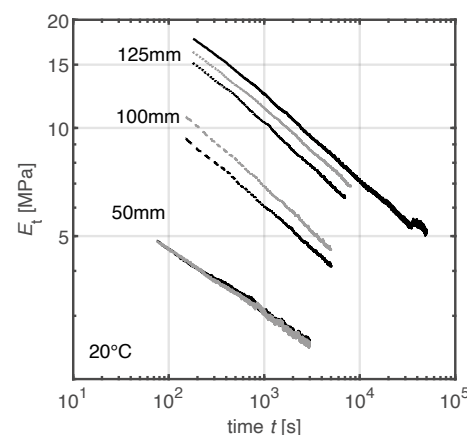
Figure 11 shows the relaxation curves at small to medium high strain levels. As already seen in Figure 3, in this strain level range, higher strain levels lead to softer material behaviour (lower stiffness).

## 4 Time-Strain and Time-Temperature Superposition Principles

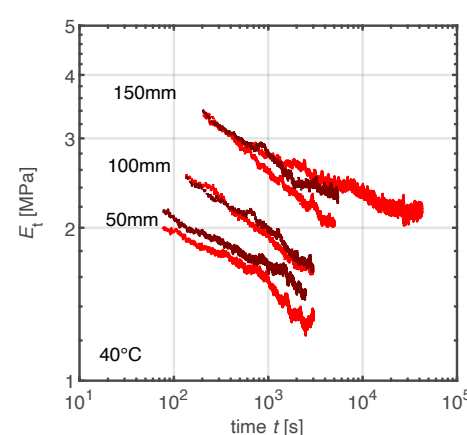
The Time-Temperature Superposition from the linear viscoelastic experiments is used without any further modification. To define a Time-Strain Superposition for the investigated



(a)



(b)



(c)

Fig. 10: Large strain relaxation tests:  $E_t(t)$  at (a) 0°C, (b) 20°C and (c) 40°C.

material, the test results were shifted horizontally as well as vertically. First, the results of the large and small/medium tests are shifted separately. Then the results are evaluated together.

### 4.1 Large strain data

#### 4.1.1 Time-Strain Superposition Principle

The individual relaxation curves overlap in their y-axis. Hence they were shifted purely horizontally with Matlab (see Eq. (8)) in order to create mastercurves.

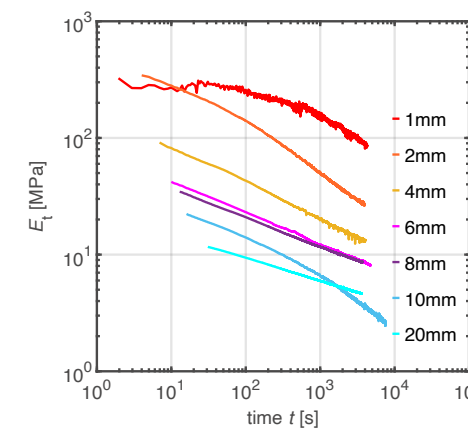


Fig. 11: Small to medium relaxation tests: true tensile modulus  $E_t$ .

For all three investigated temperatures, 50mm was chosen as reference deformation, see Figure 12. The applied shift factors are shown in Figure 13.

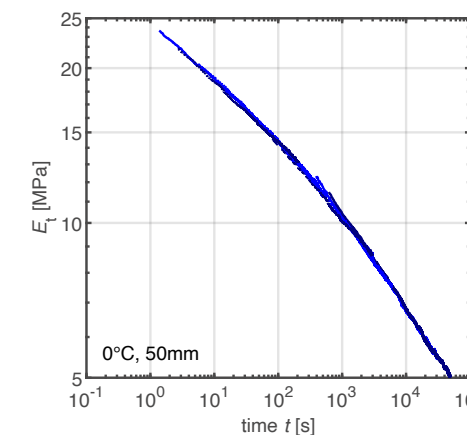
Since relatively smooth mastercurves are obtained for all three temperatures, it is assumed that the Time-Strain Superposition Principle holds for these experiments. However, since higher deformations resulted in higher stiffness, the relaxation curves at higher strain levels had to be shifted to shorter times  $t$ . This contradicts Knauss and Emris free volume theory, which states that high strains cause high free volume, which in turn accelerates the relaxation process [7].

### 4.1.2 Time-Temperature Superposition Principle

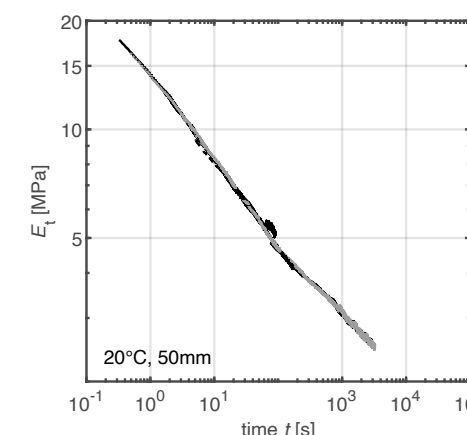
After mastercurves were successfully generated at 50mm reference displacement for all three temperatures, the TTSP from [18] was used to shift the 0°C and 40°C mastercurves to 20°C and compare them with the linear viscoelastic Prony series, which was determined with the raw data from [18], (Figure 14). Unfortunately, no continuous mastercurve is obtained. Especially between the 0°C and 20°C curves, a vertical gap appears.

### 4.1.3 Comparison with linear viscoelastic Prony series

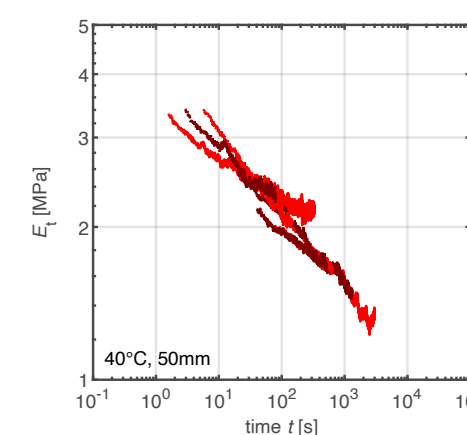
The comparison of the shifted data with the linear viscoelastic Prony series (Figure 14) shows large deviations in shape and magnitude. It should be noted, however, that the reference displacement of 50mm does not correspond to the exact same reference strain at all temperatures (see Table 1), which may lead to slight deviations. Additionally, the Prony series was determined with DMTA in plate-plate mode and had to be transformed into the tensile mode by applying Eq. (7), which is only a rough approximation. Moreover, the DMTA was conducted with samples that were stored



(a)



(b)



(c)

Fig. 12: Large strain relaxation tests: Horizontally shifted  $E_t(t)$  at (a) 0°C, (b) 20°C and (c) 40°C.

in drying beads while the Becker tensile bars were exposed for several hours to a relative humidity of 50%rH prior testing. These reasons only allow a qualitative comparison of the large strain tensile relaxation tests with the linear viscoelastic Prony series.

To explain the change in shape of the curve between the linear viscoelastic Prony series and the 50mm - 20°C nonlinear viscoelastic mastercurve, the linearity limits are considered. While a low stiffness in the linear viscoelastic range leads to a high linearity

limit, a high stiffness in the linear viscoelastic range results in a low linearity limit. Hence, a relaxation test at high temperature with a certain strain level is closer to the linear range than the same relaxation test at low temperatures. Accordingly, the test results at higher temperatures are expected to be closer to the linear viscoelastic Prony series. It can be observed that the 0°C and the 40°C curves seem to be mainly vertically offset from the linear viscoelastic Prony series. This can be explained by the fact, that the 0°C data lies in the energy elastic and the 40°C data lies in the entropy elastic range, where the linear viscoelastic stiffness is varying only slightly (compared to the glass transition range). Considering the 20°C curve, a major change in the shape compared to the Prony series is observed. The 20°C data is within the glass transition range, where large variations of the linear viscoelastic stiffness and linearity limit occur. Accordingly, the curve is far in the nonlinear range at the beginning and slowly approaches the linear viscoelastic Prony series with increasing time.

#### 4.2 Small to medium strains

##### 4.2.1 Time-Strain Superposition Principle

Figure 15(a) shows the horizontally shifted small to medium strain level relaxation curves for a reference displacement of 1mm. In Figure 15(b), the results from the large strain relaxation tests are also included. A certain similarity to the linear viscoelastic Prony series can be observed for short times. For longer times, however, greater deviations occur. Additionally, the shape of the large strain mastercurve is clearly different from the rest. The applied shift factors are shown in Figure 16.

##### 4.2.2 Additional vertical nonlinearity functions

Since it was not possible to generate a continuous mastercurve by purely horizontally shifting the individual relaxation curves, it is likely that besides the relaxation times, additional adaptations of the model are necessary. Looking at the generalized Maxwell model (Figure 1), adaption of the time invariant part  $E_{\infty}$  and of the transient part  $\Delta E$  as a function of the applied strain level is possible. In Schapery's model, this can be considered with the nonlinearity functions  $h_{\infty}(\epsilon_t)$  resp.  $h_0(\epsilon_t)$  and  $h_{1,2}(\epsilon_t)$  resp.  $h^*_{1,2}(\epsilon_t)$ . Schapery generally suggests to split the relaxation function into a time invariant and a transient part, and to determine  $h_{\infty}(\epsilon_t)$  resp.  $h_0(\epsilon_t)$  by evaluating solely the time-invariant part and  $h_{1,2}(\epsilon_t)$  resp.  $h^*_{1,2}(\epsilon_t)$  by evaluating solely the transient part.

It was decided to do the further evaluation with  $E_{0,\epsilon}$  and  $h_0$ , since the relaxation tests are too short to adequately determine  $E_{\infty,\epsilon}$ . However,

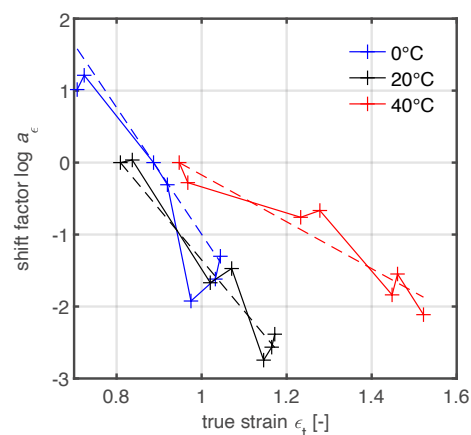


Fig. 13: Horizontal shift factors to create mastercurves at a reference deformation of 50mm. The dashed lines correspond to linear approximations.

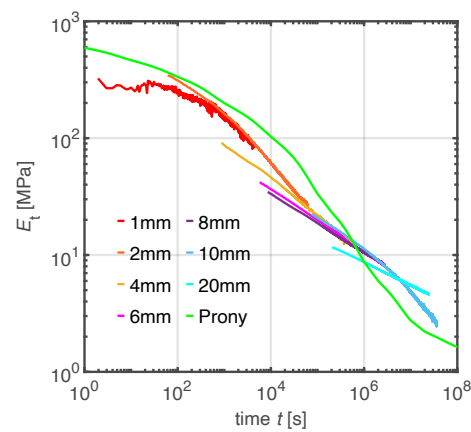


Fig. 14: Application of the Time-Temperature Superposition Principle in order to shift the 50mm mastercurves to a reference temperature of 20°C and comparison with Prony series (3G(t)). The WLF parameters [18] were used.

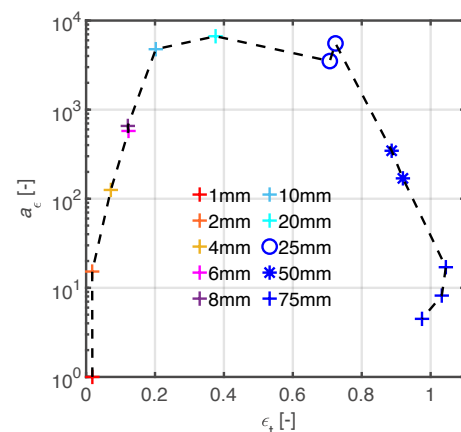


Fig. 15: Horizontal shift factors to create mastercurves at a reference deformation of 1mm.

curves (log-log curves) vertically upward and to the left as the strain increases. It is not necessary to change the shape of the individual log-log relaxation curves. Hence,  $h = h_0 = h^*_{1,2}$  is assumed, which fits the previous observation of approximately constant linearity limits at 0°C. After dividing the relaxation curves by  $h$ , a mastercurve can be generated only by horizontal shifting. The  $h$ -values were determined manually with a trial-and-error procedure. Figure 17(a) represents the relaxation curves divided by  $h$ . The corresponding  $h$ -values are shown in Figure 17(b). The final mastercurve, which is obtained by horizontally shifting the individual  $E(t)/h$ -curves, is presented in Figure 17(c) and the corresponding shift factors in Figure 17(d). Compared to Figure 15(c), a much more continuous mastercurve is obtained. However, large deviations from the linear viscoelastic Prony series are still present. The reason for this still has to be clarified.

Figure 18 shows that the course of  $h$  has

similarities to the course of  $E_{11x t_0}$  resp.  $E_{t_0}$ , wherein  $t_0$  is the time at which the relaxation test starts.

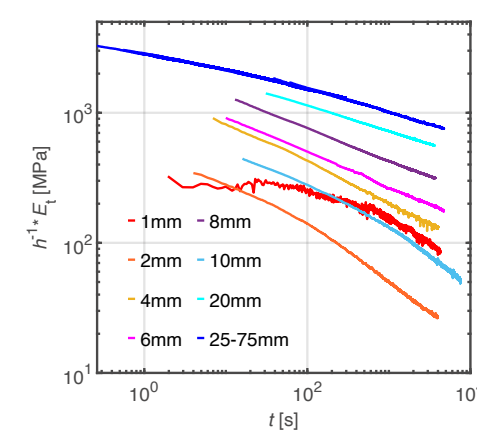
## 5 Summary and outlook

In this paper the nonlinear viscoelastic material behaviour of PVB (Saflex® RB41 [16]) was investigated in uniaxial relaxation tests at various strain levels reaching from small/medium to large. The large strain level relaxation tests were performed at three different temperatures. The lowest temperature was 0°C, which is below the glass transition range of the investigated material. The highest temperature (40°C) exceeds the glass transition range and the third temperature (20°C) lies in the range of the glass transition. By shifting the individual relaxation curves horizontally, mastercurves for a reference displacement of 50mm were successfully created for all three temperatures, which speaks for the existence of a TTSP. Subsequently, TTSP was used to shift the 50mm mastercurves to a reference temperature of 20°C. It was found that the shape of the nonlinear viscoelastic relaxation curve differs considerably from the linear viscoelastic Prony series. At short times, the nonlinear viscoelastic relaxation modulus is significantly smaller than in the linear case. With increasing time, however, the nonlinear viscoelastic relaxation curve approaches the linear viscoelastic Prony series.

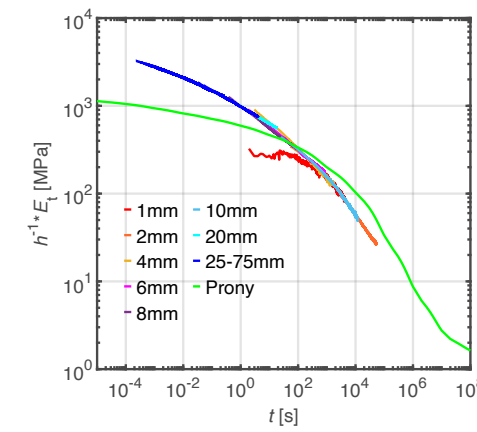
At a temperature of 0°C, true strain levels from  $\approx 0.5\%$  - 105% have been considered. Initially, spring stiffnesses (defined here as secant moduli) decrease at small to medium strains but increase at very large strains. TTSP was applied to generate a mastercurve. It was found that better results are obtained (most continuous mastercurve) when the individual curves are shifted horizontally and vertically. Consequently, both the springs and dampers of the generalized Maxwell model are dependent on the applied strain level. The vertical shift factor can be derived from the true tensile modulus at the beginning of the relaxation test  $E_{t_0}$ . Large strain levels were shifted to shorter times, which contradicts the free volume theory.

The investigations carried out in this paper are to be interpreted as preliminary test results and require validation. Further research is absolutely needed in order to understand the mechanical behaviour of PVB under large deformations. The following points need clarification:

- What is the origin of the vertical offset between the 0°C and 20°C curves after applying the TTSP? Is the TTSP still valid for PVB interlayer in the nonlinear viscoelastic range?



(a)



(c)

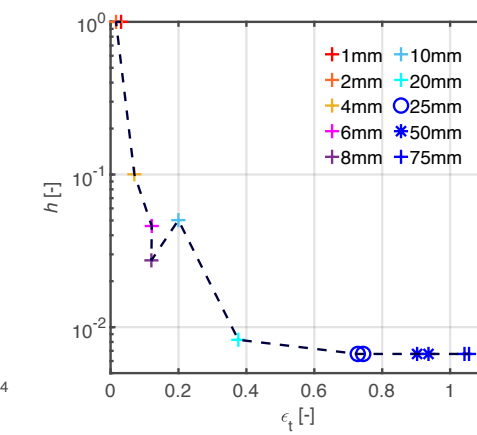
Fig. 17: (a)  $h^{-1}E_t(t)$ : vertically shifted relaxation curves, (b) vertical shift factors  $h$ , (c)  $h^{-1}E_t(t)$  horizontally shifted, (d) horizontal shift factor  $a_{\epsilon}$ .

- How big is the influence through a different moisture content?

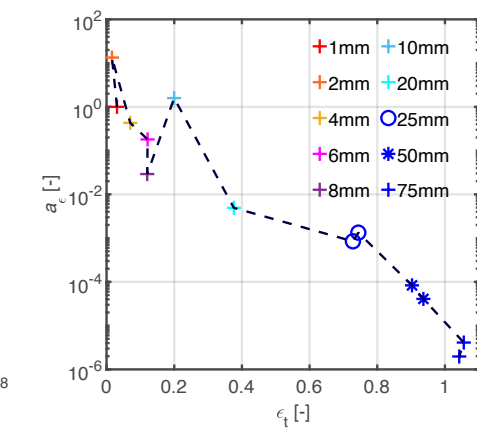
Additionally, it is suggested to further increase the experimental data base of the relaxation tests. The following tests are recommended:

- Uniaxial relaxation tests in the linear viscoelastic range at various temperatures, to generate a linear viscoelastic mastercurve in tensile mode and with the same moisture content than the nonlinear viscoelastic tests.
- Uniaxial relaxation tests at a constant strain level (in the nonlinear viscoelastic range) and at various temperatures (e.g., in 2.5°C steps) to check the validity of the TTSP.
- Uniaxial relaxation tests at 20°C with various strain levels to confirm that the Prony series is reached after a certain time.
- Uniaxial relaxation tests with higher displacement rate to reach the strain level. The faster, the better, since  $E_0$  can be better approximated in this way.

Furthermore, it is recommended to compare all data where the linearity limit is exceeded to a similar extent.



(b)



(d)

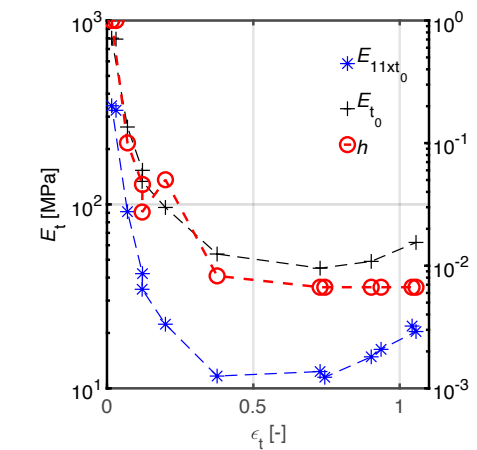


Fig. 18: Comparison of vertical shift factor  $h$  with  $E_{11x t_0}$  (first evaluation point) and  $E_{t_0}$  (begin of relaxation test).

## 6 Acknowledgement

The authors would like to thank the former master student Bianca Farr for the support with the execution and evaluation of the large strain relaxation tests as well as Eastman Chemical Company for providing the test samples.

## References

- [1] Richard Allan Schapery. A theory of non-linear thermoviscoelasticity based on irreversible thermodynamics. American Society of Mechanical Engineers New York, NY, 1966.
- [2] Richard Allan Schapery. Further development of a thermodynamic constitutive theory: stress formulation. Purdue University School of Aeronautics, Astronautics and Engineering Sciences, 1969.
- [3] Richard Allan Schapery. "On the characterization of nonlinear viscoelastic materials". In: *Polymer Engineering & Science* 9.4 (1969), pp. 295-310.
- [4] Wolfgang Gustav Knauss and IJ Emri. "Non-linear viscoelasticity based on free volume consideration". In: *Computational Methods in Nonlinear Structural and Solid Mechanics*. Elsevier, 1981, pp. 123-128.
- [5] Thomas W Strganac et al. "Characterization of nonlinear viscoelastic behavior using a dynamic mechanical approach". In: *AIAA journal* 33.5 (1995), pp. 904-910.
- [6] James L Rand, John K Henderson, and Debora A Grant. "Nonlinear behavior of linear low-density polyethylene". In: *Polymer Engineering & Science* 36.8 (1996), pp. 1058-1064.
- [7] Jan Kolarik and Alessandro Pegoretti. "Non-linear tensile creep of polypropylene: Time-strain superposition and creep prediction". In: *Polymer* 47.1 (2006), pp. 346-356.
- [8] Hal F Brinson, L Catherine Brinson, et al. *Polymer engineering science and viscoelasticity. An introduction*. Springer, 2008.
- [9] Didier Delince et al. "Post-breakage behaviour of laminated glass in structural applications". In: *Conference on Architectural and Structural Applications of Glass*. IOS Press, 2008, pp. 459-467.
- [10] Eyad Masad et al. "Nonlinear viscoelastic analysis of unaged and aged asphalt binders". In: *Construction and Building Materials* 22.11 (2008), pp. 2170-2179.
- [11] Florian Becker. "Entwicklung einer Beschreibungsmethodik für das mechanische Verhalten unverstärkter Thermoplaste bei hohen Deformationsgeschwindigkeiten". PhD thesis. Martin-Luther-Universität Halle-Wittenberg, 2009.
- [12] Johannes Franz et al. "Investigation of the post-breakage behavior of laminated glass: Through-Cracked-Tensile test". In: 83 (Apr. 2014), pp. 241-252.
- [13] Johannes K Kuntsche. "Mechanisches Verhalten von Verbundglas unter zeitabhängiger Belastung und Explosionsbeanspruchung: Mechanical behaviour of laminated glass under time-dependent and explosion loading". PhD thesis. Technische Universität Darmstadt, 2015.
- [14] Miriam Schuster et al. "Investigations on the thermorheologically complex material behaviour of the laminated safety glass interlayer ethylene-vinylacetate". In: *Glass Structures & Engineering* 3.2 (2018), pp. 373-388.
- [15] Johannes Kuntsche, Miriam Schuster, and Jens Schneider. "Engineering design of laminated safety glass considering the shear coupling: a review". In: *Glass Structures & Engineering* 4.2 (2019), pp. 209-228. issn: 2363-5142 2363-5150. doi: 10.1007/s40940-019-00097-3.
- [16] Eastman Chemical Company. Product technical data Saflex® Clear (R series) - Polyvinyl Butyral Interlayer. English. 2020.
- [17] Correlated Solutions, Inc. Vic-Gauge 2D/3D. 2021. url: <http://www.isisys.com/vic-gauge-2d3d/> (visited on 10/15/2021).
- [18] Miriam Schuster, Kerstin Thiele, and Jens Schneider. "Investigations on the viscoelastic material behaviour and linearity limits of PVB". In: *Engineered transparency international conference at Glasstec*. 2021.
- [19] STAEDTLER Mars GmbH & Co. KG. Lumocolor® non-permanent pen 311. 2021. url: <https://www.staedtler.com/de/de/produkte/marker/fohlenstifte/lumocolor-non-permanent-pen-311-non-permanentuniversalstifts-m311/> (visited on 10/15/2021).
- [20] The MathWorks, Inc. Matlab R2020a. 2021. url: <https://www.mathworks.com/help/releases/R2020a/index.html> (visited on 10/15/2021).
- [21] Testing of plastics; stress relaxation test. withdrawn Standard. DIN Deutsches Institut für Normung e. V., 1984-01.
- [22] Glass in building – Laminated glass and laminated safety glass – Determination of interlayer viscoelastic properties, German version. Standard. DIN Deutsches Institut für Normung e. V., 2020-01.